



EIDESSTATTLICHE ERKLÄRUNG

Ich erkläre an Eides statt, dass ich die vorliegende Arbeit selbstständig verfasst, andere als die angegebenen Quellen/Hilfsmittel nicht benutzt, und die den benutzten Quellen wörtlich und inhaltlich entnommenen Stellen als solche kenntlich gemacht habe. Das in TUGRAZonline hochgeladene Textdokument ist mit der vorliegenden Masterarbeit identisch.

Datum

Unterschrift

Inhaltsverzeichnis

Introduction.....	3
Material and Methods.....	7
Confocal Laser Scanning Microscopy	7
BodiPY.....	7
Er-Tracker-Red.....	8
Mito Tracker Deep Red	8
Hoechst 33342.....	8
HCS LipidTOX Deep Red.....	8
Vectrashield with DAPI.....	9
Fixation	9
Long Term Live Cell Imaging.....	9
CellLight Probes.....	9
Cell Culture	10
Growth Curve Experiments	10
BSA Fatty Acid Conjugates.....	10
Image Analysis.....	11
Lipid Droplet Analysis	11
Growth Curve Analysis	14
Statistical analysis.....	16
Results	17
Lipid Loading.....	17
Growth Curves.....	19
Long Term Live Cell Imaging.....	20
Discussion	26

Conclusion and Perspectives	28
Acknowledgements	30
Literaturverzeichnis	30

Introduction

The number of people diagnosed with chronic liver diseases or cirrhosis every year, is steadily increasing in the 21st century. America's Centers for Disease Control and Prevention published data from the year 2015 showing that 3.9 million Americans were diagnosed with chronic liver disease or cirrhosis, i.e. 1.6% of the American population (Centers for Disease Control and Prevention 2016). That year 40,326 patients died, resembling an overall death rate of 12.5 people out of 100.000. Whilst the death rate in America seems to be stable or even declining, it is a completely different story especially for underdeveloped countries. The World Health Organisation reported for the year 2012 death rates due to cirrhosis all around the world (World Health Organisation). The world average was 25.7 people out of 100.000 reaching beyond the hundreds in countries like Sierra Leone, Guyana and Egypt; for the sake of comparison the rate in America was 11 or 14.55 in Austria respectively. Causes for cirrhosis are plentiful, but predominantly alcohol abuse, viral hepatitis, pharmaceuticals, autoimmune diseases and congenital diseases (Clark und Diehl 2003; Rinella 2015). However, large proportions are so called cryptic cirrhosis cases, i.e. cases without an obvious cause. In the last years, a term first defined in the 1980's has gained more and more attention, the non-alcoholic fatty liver disease (NAFLD). NAFLD is thought to be the leading culprit for a major part of the cryptic cirrhosis cases, but is itself poorly understood. NAFLD is divided into two subgroups, non-alcoholic fatty liver (NAFL) and non-alcoholic steatohepatitis (NASH). It occurs in every age group and ethnicity and is found in 14%-30% and 5%, respectively, of the population. Individuals with NAFLD will most likely not display any symptoms, in the case of NAFL there are only mild interspersed segments of inflammation in addition to the accumulation of fat. If the inflammation becomes more severe, NAFL turns into NASH, which then can lead to fibrosis, culminating as a final stage in cirrhosis, but more often than not the inflammations will recede and turn into NAFL again (FIG.1). The chance for a case of NAFL to propagate into live threatening cirrhosis is quite low. Our understanding of the underlying mechanism is poor; but the following risk factors for developing NAFLD have been identified: obesity, hypertension, dyslipidaemia, type 2 diabetes and metabolic syndrome, all on the rise in today's world population.

With an already high prevalence and the likelihood of becoming an even greater problem in the future, scientists all around the world are searching for a way to better diagnose,

understand and fight NAFLD. The only method to certainly diagnose NAFLD is still a liver biopsy, a method unthinkable for a routine control check-up. Sonography, a widely available diagnostic technic, has a high sensitivity, but only after the fat content of the liver reaches a level of 33%. The only imaging techniques that can accurately measure the fat content are Magnetic Resonance Imaging and Magnetic Resonance Spectroscopy. But availability of those machines is low since they are quite expensive, and moreover they cannot differentiate between NAFL and NASH. The search for biomarkers has led to identification of the enzyme alanine aminotransferase, but it rather seems to indicate insulin resistance in patients with NAFLD instead of indicating it in the first place. As of today, treatment consists of combating the before mentioned risk factors with lifestyle changes, antioxidants and glucose sensitizing agents (Adams und Angulo 2006).

There are two main questions research has to address, first how to easily diagnose the presence of NAFLD as early as possible and second, to understand the molecular mechanism of the disease to find potential targets for a cure. Some scientists suggest a two hit theory. The accumulation of fat in the liver, to a certain extent is not harmful. The liver is the central organ for fat and energy traffic in humans and needs fat reserves to ensure a healthy metabolism (Campbell et al. 2012; Horton et al. 2008; Penzlin und Beinbrech 2009; Rutkowski et al. 2015). But if the fat content reaches a certain level a, second hit can kill the cells.

If there is surplus amount of fatty acids available than needed for biosynthesis of membranes or protein acylation, it will be stored in lipid droplets for later use or burned in a process called beta-oxidation. This process takes place in the matrix of mitochondria, an organelle specialized on energy production. The products of beta-oxidation are reducing agents and acetyl-CoA. The latter is further metabolized in the citric acid cycle, again into more reducing agents. All of those can be used to power the complexes of the electron transport chain to generate ATP in the process called oxidative phosphorylation. If this process is slightly imbalanced, electrons can jump back from succinate, associated to complex two of the electron transport chain, to NAD^+ in a phenomenon called reverse electron transfer (RET). This is accompanied by a generation of reactive oxygen species (ROS) (Schönfeld et al. 2010; Speijer et al. 2014). Elevated ROS levels are toxic for the cell, primarily

damaging mitochondria irreversibly, thus promoting apoptosis, a process of coordinated cell death. To slow down ROS generation, the mitochondrial system, normally highly connected, starts breaking down into many smaller fragments concomitantly decreasing its energy output (Scott und Youle 2010; Karbowski 2010; Archer 2013). If this is still not enough to prevent mitochondrial damage which cannot be repaired by a process termed mitophagy (i.e. the removal of damaged mitochondria by controlled self-digestion (autophagy)), the cell will undergo apoptosis. Like in any tissue the liver displays a constant turnover of cells, but the fine structure of cords and sinusoids can be damaged fast and irreversibly, as is the case in fibrosis.

in order to obtain a better understanding of the molecular mechanisms leading to liver disease the objectives of my thesis were to investigate effects of different fatty acids on liver cells, especially on growth including determination of toxicity levels, on steatosis (lipid droplet accumulation) and mitochondrial dynamics. To determine fatty acid dependent effects the two major mammalian fatty acids oleic acid, a singly unsaturated long chain fatty acid (C18:1), and palmitic acid, a saturated long chained fatty acid (C16:0), were employed in this study. I will first introduce you into how I induced steatosis in the human HepG2 liver cell line and measured their lipid droplet content. Secondly, I will present the results of the growth curve experiments. And finally I will discuss the results of the long term live cell imaging in consideration of the before mentioned stress factors.

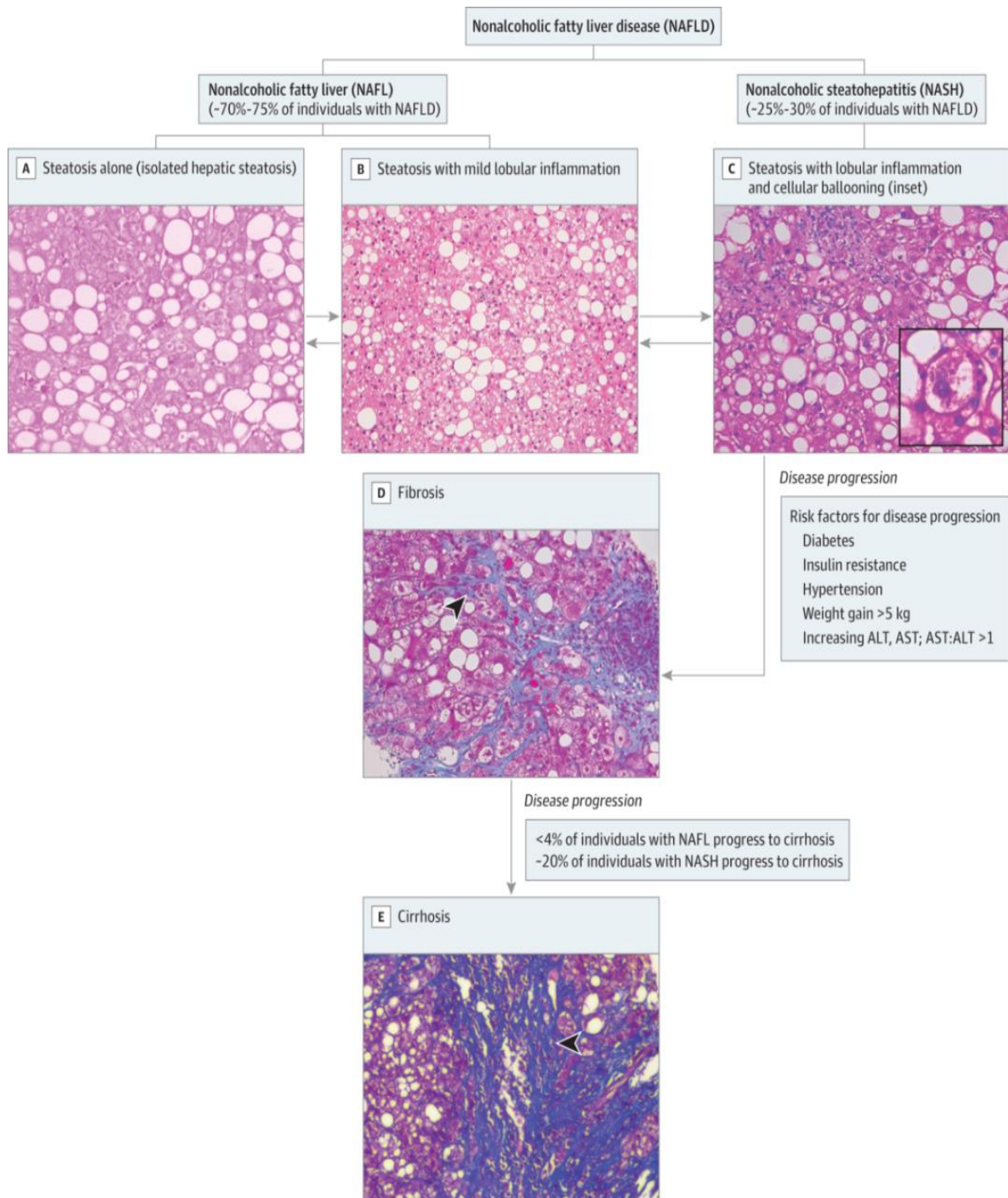


Figure 1 Histologic samples showing the cellular defects and schematic progression of NAFLD. Except the cirrhosis all of the previous steps have no negative effect on liver activity and are thus hard to diagnose. The latent accumulation of fat without any inflammation, here shown as NAFL A. (Rinella 2015)

Material and Methods

Confocal Laser Scanning Microscopy

I used the Nikon A1 confocal laser scanning microscope (CLSM) to work on fixed and living cells. This type of microscope has several advantages over a traditional wide field fluorescence microscope, which go hand in hand with drastic alterations to the design of the instrument. One of the name giving factors of “confocal” microscopy is the addition of a pinhole in front of the detector, which prohibits most out of focus fluorescence to reach the detector. This simple addition results in images that are much crisper and allows us, in theory, to acquire just a single plane of interest of the specimen in question. The most extensive modification in comparison to a normal compound microscope is the scanning laser detection method. In such a microscope at no point in time a magnified image of the specimen exists that could be detected with an eye or camera. The laser scans the specimen a point at the time, and a single detector, simplest would be a photomultiplier tube (PMT), is used to generate a current corresponding to the photons emitted at said time point. The computer then calculates an intensity value out of the generated current, and displays each time point as a pixel with a certain grey level corresponding to the intensity. So without a computer one would never be able to get an image out of a laser scanning microscope. The images of those microscopes are also colourless; all the beautiful multicolour pictures published, are colorized via the use of defined look up tables (LUT). All these modifications bring again the benefit of reducing the illumination of undesired areas of our specimen and a very sensitive detection, improving the overall resolution. Combining multiple pinholes with the laser scanning illumination technology, results in detailed and crisp images without the need to perform biased image improving methods like deconvolution. Another profit of the acquisition of defined z planes lies in the possibility for easy 3 D reconstruction.

BodiPY

The fluorescent dye Bodipy is a neutral lipid analogue, which easily permeates cellular membranes and accumulates in LDs. It is not 100% specific for LDs since to some extent it also labels membranes. But if the used concentration is not too high the specific fluorescence is easily distinguishable from the background. The high quantum yield of the dye, as well as the simple use, makes this dye extremely easy to work with. Its fluorescence

is settled in the green part of the spectra (493/503). Staining with a 1:1000 dilution of the stock solution (10mg/ml) directly in the culture media and incubating them for 5 minutes results in distinct stains of LDs in most cell lines (Johnson 2010).

Er-Tracker-Red

The mode of action of the ER-Tracker is completely different from that of Bodipy although it is a Bodipy fluorophore coupled to a glyburide molecule that shows high specificity for the ATP dependent K⁺ channels associated with the endoplasmic reticulum. The wavelength of the fluorophore is also shifted into the red spectra (587/615) (Johnson 2010).

Mito Tracker Deep Red

All Mito Tracker dyes are mitochondria selective probes. The common mode of action of all those dyes is that they are neutral molecules at the point of application which allows them to permeate freely through membranes. In mitochondria those dyes accept protons and become fluorescent. After the protonation they cannot leave the mitochondria anymore which leads to their accumulation in metabolic active mitochondria. This type of Mito Tracker also has the ability to form thiol bonds with proteins, which makes them fixable. The excitation and emission spectra is settled on the far red side of the spectra (644/665) (Johnson 2010).

Hoechst 33342

Hoechst is a fluorescent dye with characteristics similar to the more often used DAPI. It interchelates into dsDNA and has similar excitation and emission spectra (350/461). The biggest difference is that Hoechst can easily permeate through the membrane of living cells (Johnson 2010).

HCS LipidTOX Deep Red

Is also a neutral lipid stain but can only be used on previously formaldehyde fixed cells. It is the only dye that is available with a far red spectrum (637/655). I used it only as an alternative for Bodipy, if I needed the green wavelength for the Cell light Probes (Johnson 2010).

Vectrashield with DAPI

Vectrashield is a mounting media specialized for fluorescent microscopy buffering bleaching to a certain extent. This mounting media also contains DAPI, 4',6-diamidino-2-phenylindole, a DNA intercalating minor groove binding fluorescent dye. This dye is a widely use nuclear stain with a blue emission (358/461). Though DAPI can permeate the membranes of living cells, the amount needed to do so is quite high, so it is basically only used for fixed samples. This nuclear co-stain was used to automatically calculate the number of cells present in each image.

Fixation

Cells were fixed using a 3,7% formaldehyde solution in 1x Phosphate-Buffered-Saline (PBS). After the cells had been incubated for 5 minutes with Bodipy, the prewarmed Formaldehyde solution was added and returned to the incubator for 10 Minutes. Prior to the embedding the cells were washed two times with PBS.

Long Term Live Cell Imaging

For the twenty-four-hour experiments I was able to use a spinning disc system. Those systems lack resolution, especially in the z axis, but instead give you improved acquisition speed. The laser beam with the Yokugwa total illumination micro lens system gets split into multiple beams and pinholes, reducing also the overall exposition and phototoxic effects. Acquisition with a spinning disk system is also possible with a normal CCD or CMOS camera, implying that a real image is present. The special micro lens system of the Yokugawa spinning disk system in theory increases the light gain tenfold allowing working with a relative intensity of the 546nm NeHe Laser (5mW max.) of 5% during the mitochondrial imaging. Cells were seeded 24 hours prior to the experiment in a glass bottomed well dish and transfected with cell light probes (Springer und Pawley 2006).

CellLight Probes

I used two different kinds of cell light probes during the experiments, mitochondria-RFP and ER-GFP. The fusion constructs use special leader sequences to ensure that they arrive at their right destination. In case of the mitochondrial probe the leader sequence in use is the E1 of the Alpha pyruvate dehydrogenase coupled with TagRFP, resulting in a mitochondrial labelling that is independent of the membrane potential. The ER probe is a fusion construct

of the ER signal sequence of calreticulin with KDEL and emGFP. The virus in which those constructs are packaged is the insect baculovirus. This virus can enter into mammalian cells but is unable to replicate in them, leading to a transient expression but little adverse side effects. Absorption and emission spectra for mitochondria-RFP are (555/584) and for ER-GFP (488/510) (Johnson 2010).

Cell Culture

HepG2 cells were cultivated in RPMI 1640 with standard glucose concentration, 2g/l, and 4mM glutamine. The population at the start of the experiments was heterogeneous, containing cells that were more than double the size of normal HepG2 cells, around 50µm. To get rid of these giants, a FACS sorting was performed. So clone 1-9 refers to single cell clones whereas the mixture of giants and the normal sized cells is named the parental line.

Growth Curve Experiments

Growth curve analysis was performed using a Zeiss Cell Observer microscope. Twelve-well plates were seeded with 100,000 cells and the media was not changed during the experiment. Images were acquired at five times magnification using phase contrast every two and a half hours. With the multidimensional acquisition tool, a time series was coupled with multiple positions within each well.

BSA Fatty Acid Conjugates

To induce steatosis BSA-FA conjugates were used for better solubility and thus improved cellular uptake. The molar ratio of the solution from sodium palmitate or sodium -oleate to BSA was 6:1. The BSA solution was prepared using 2.26g of FA-free BSA dissolved in 100ml of 150mM NaCl solution at approximately 37 °C. 30.6mg of sodium palmitate or 33.4 mg of sodium oleate were dissolved in 44ml of a 150mM NaCl solution at 70°C. 50 ml of the BSA solution were set aside and diluted 1:1 with 15mM NaCl solution to create a 0.17 mM BSA control stock. To the remaining BSA solution 40ml of the hot FA solution was added; this step had to be performed fast, if the FA was allowed to cool it precipitated. The conjugate solution was stirred at 37°C for one hour; afterwards the volume was adjusted to 100ml and the pH to 7.4 (Seahorse Bioscience 2010).

Image Analysis

All the analyses were performed with the open source software package FIJI vers. 1.51h (FIJI is just ImageJ). Using the own language of the program I compiled scripts for the analyses facilitating the work by reducing the time spent with manual input to a minimum (Schindelin et al. 2012).

Lipid Droplet Analysis

Provided here is the code in .ijm language used for the analysis of all the z-stacks acquired. Highlighted in yellow are the file endings which must be manually adjusted to the input. Step 1 sets the general parameters which are going to be measured. This step is essential because the program refers to columns in other tables than the primary results table just as numbers and not with their names. Step 2 gets the name of the image and rids of the file ending. Step 3 opens an information popup for the user how the channels have to be arranged for the program to work as intended and opens the channel arrangement tool. In step 4 we duplicate the cropped starting image and perform a maximum intensity z-projection on one of them, giving an easy overview of the three dimensional sample. In step 5 we define a region of interest (ROI) that is going to be analyzed further. This allows for the manual exclusion of clipped cells or fluorescent crystals in the media. Step 6 returns to our starting image and applies the same ROI we defined before, crops it and splits the two channels for further analysis. Step 7 is the treatment of the channel containing the nucleus stain. After a z-projection the image is converted into the binary format. The commands "Fill Holes" and "Watershed" are used to compensate partially for a bad signal and to separate stacked nuclei. Nuclei on edges are excluded as well as too small particles. Step 8 is the analysis performed on the LD channel. A z-projection is followed by an automated thresholding step. The use of an algorithm abolishes on one side the need of a manual input and makes the results also reproducible. Step 9 selects the Summary window containing all the compiled information of the LD analysis and defines the lines and columns to be read. Step 10 just selects the window containing the nucleus information and shows us the result of the automated cell counting. This is important because step 11 now creates a log entry and asks the user if the automated count was performed correctly or if an adjustment is desired. The log entry always contains both numbers and can be saved as a text or excel file. The final step 12 just clears up everything before the next image is analyzed.

1. `run("Set Measurements...", "area mean standard redirect=None decimal=3");`
2. `title=getTitle;`
`dotIndex=indexOf(title, ".");`
`name=substring(title, 0, dotIndex);`
3. `waitForUser("Please arrange channels to following Order: \n CH1: Nucleus Stain \n CH2: LD Stain \n DELETE all other channels.");`
`run("Arrange Channels...");`
4. `run("Duplicate...", "duplicate");`
`selectWindow(name+"-1.nd2");`
`Stack.setDisplayMode("composite");`
`run("Z Project...", "projection=[Max Intensity]");`
5. `run("ROI Manager...");`
`setTool("rectangle");`
`waitForUser("Select cell for analysis");`
`roiManager("add")`
`close()`
`selectWindow(name+"-1.nd2");`
`close()`
7. `selectWindow(title);`
`roiManager("select",0)`
`run("Crop");`
`run("Split Channels");`

```
selectWindow("C1-"+title);

run("8-bit");

run("Z Project...", "projection=[Max Intensity]");

selectWindow("C1-"+title);

close()

selectWindow("MAX_C1-"+title);

run("Make Binary");

run("Fill Holes");

run("Watershed");

run("Analyze Particles...", "size=25-Infinity show=Nothing display exclude
summarize");

selectWindow(name+"-1.nd2");
```

8.

```
selectWindow("C2-"+title);

run("8-bit");

run("Z Project...", "projection=[Max Intensity]");

selectWindow("C2-"+title);

close()

selectWindow("MAX_C2-"+title);

run("Auto Threshold", "method=MaxEntropy white");

run("Analyze Particles...", "size=0-Infinity show=Nothing display summarize");
```
9.

```
selectWindow("Summary");

lines = split(getInfo(), "\n");
```

```

headings = split(lines[0], "\t");

nuclei = split(lines[1], "\t");

LD = split(lines[2], "\t");

10. selectWindow("MAX_C1-"+title);

print(name, " ", "LD Vol.," " ", LD[2], " ", "Nuclei Automated Count", "
", nuclei[1], " ", "Nuclei User Input", " ", getNumber("Correct nucleus count if
necessary", nuclei[1]));

12. run("Clear Results");

roiManager("delete")

selectWindow("Summary");

run("Close")

selectWindow("MAX_C2-"+title);

close()

selectWindow("MAX_C1-"+title);

close()

```

Provided above is the script code for FIJI in .ijm format. Besides the necessary information the user has to input via prompts, all the parts including the thresholding are automated and thus the results are reproducible. The yellow highlighted parts of the script stand for the file format you are using and must be adjusted if necessary. The output in the log window is formatted in a certain way so it could be saved as a txt-file or directly as an excel file for further evaluation and testing.

Growth Curve Analysis

The output of the analysis tool is the number of pixels for each image that are occupied by the cells. In excel a mean is generated out of all the positions in one well and the resulting values are then plotted. A linear function is calculated out of the plot data during the exponential growth phase and the maximum slope gives us then the information of how all the conditions compare to a control cells. Step 1 gets the file name without the file type

ending. Step 2 sets the parameters for the analysis and undoes any previous calibrations so that the results are shown in pixels. Step 3 is a background reduction based on the rolling ball algorithm followed by the binarization. In Step 4 the analysis is run and the summary table is defined for the readout. Step 5 creates the output log, which can be saved as a text or excel document. Step 6 resets everything before the next image is loaded.

```
1.    name=getTitle;

      dotIndex=indexOf(name, ".");

      title=substring(name, 0, dotIndex);

2.    run("Set Measurements...", "area mean standard min redirect=None decimal=2");

      run("Set Scale...", "distance=0 known=0 pixel=1 unit=pixel");

3.    run("Subtract Background...", "rolling=2");

      setOption("BlackBackground", true );

      run("Make Binary");

4.    run("Analyze Particles...", "display summarize");

      selectWindow("Summary");

      lines = split(getInfo(), "\n");

      Area = split(lines[1], "\t");

5.    print(name, " ", "Area", " ", Area[2]);

6.    run("Clear Results");

      selectWindow("Summary");

      run("Close");

      close();
```

Presented above is the code I used for the growth curve analysis in FIJI in .ijm format. This script works just as an area calculator, which measures for every time point the space taken up by the culture. Plotting this data directly generates

the growth curve. But to compensate for the variations in seeding density I did not compare the curves directly but generated a linear function and normalized the slope. For this the information from the log window can be either saved as txt-file or directly copied into excel.

Statistical analysis

All the ANOVA tests have been performed using Perseus V1.6.1.1 with the artificial Group variance of two. I used “permutation based FDR” for truncation, with an FDR of 0.05 and 250 randomizations. To identify the significant changes inside the groups a post hoc test was performed, but no information on which test specifically this analysis is based on is publically available (Perseus Software 2017).

Results

Lipid Loading

HepG2 cells were seeded on cover slips, previously treated with KOH 5%, and allowed to settle and grow for 24 hours before they were incubated with varying concentrations of FA conjugates for 24 hours. Cells were fixed and stained with BodyPI and imaged using the ZEISS LSM100. For oleic acid a concentration dependent increase of LD size could be found, seemingly reaching a point of saturation between 250 and 500 μ M (Fig.2 and Fig.3C). The individual lipid droplet volume of the cells varied greatly as can be seen from the high standard deviation. For Palmitic acid no such correlation between palmitic acid concentration in the media and lipid droplet volume could be found. Rather after a slight initial increase no further lipid droplet accumulation could be observed (Fig.3 B).

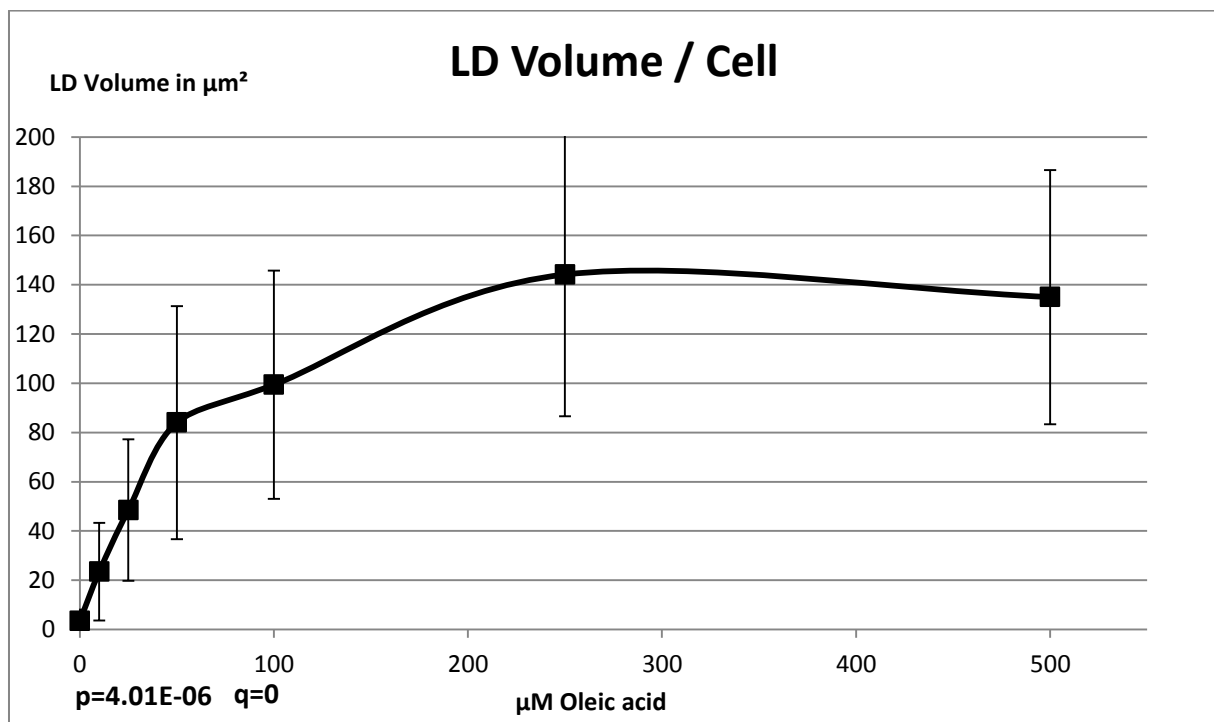


Figure 2 Shown in this plot is the positive correlation of oleic acid concentration in the media and lipid droplets accumulated in the cytosol after 24 hours. Though the standard deviation is quite high their trend to reach a saturation somewhere between 250 and 500 μ M is clearly discernible.

Using a Nikon A1 confocal laser scanning microscope I performed additional live cell imaging and discovered that even at intermediate concentrations of palmitic acid, the cells start to look much worse than their oleic acid treated counterparts (Fig.3 A).

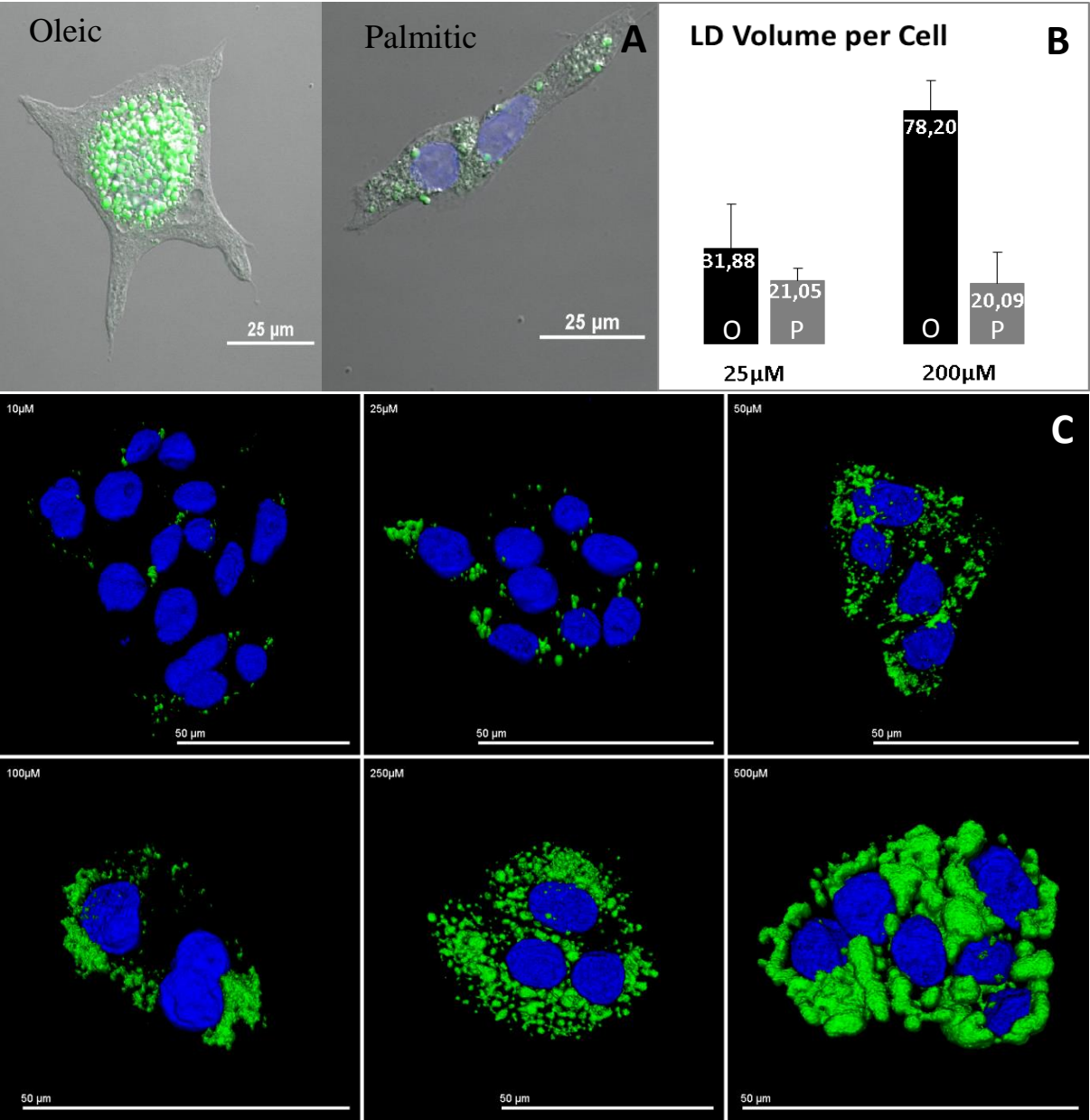


Figure 3 A) Living cells stained with BodyPI, shown in green, and Hoechst, shown in blue. When comparing cells treated with either oleic or palmitic acid at a concentration of 250 μM the cells treated with palmitic acid appear to be condensed. B) A comparison of how many lipid droplets got accumulated over 24 hours using oleic and palmitic acid. C) A surface rendering of the imaged HepG2 cells at the different concentrations of oleic acid tested. DAPI shown in blue and BodyPI in green.

Growth Curves

For the experiment HepG2 cells were seeded in 12 well plates and carefully shaken for some time in an infinity loop pattern to distribute them evenly throughout the whole well. Afterwards the plate was put into a ZEISS Cell Observer, which was programmed to take an image every hour at several positions in the well for 120 hours. I calculated the confluency score for all the images of each well, averaged and plotted them. At the exponential growth phase a linear function was fitted to the graph and the slopes were used for the actual growth speed calculations. Within each growth curve experiment I normalized all the data on the control lines and then formed means out of four replicates for the final plot. The results were ANOVA tested for significance with a falls discovery rate of 0.05. In addition a post hoc test was performed to identify the significantly variant concentrations from the control line.

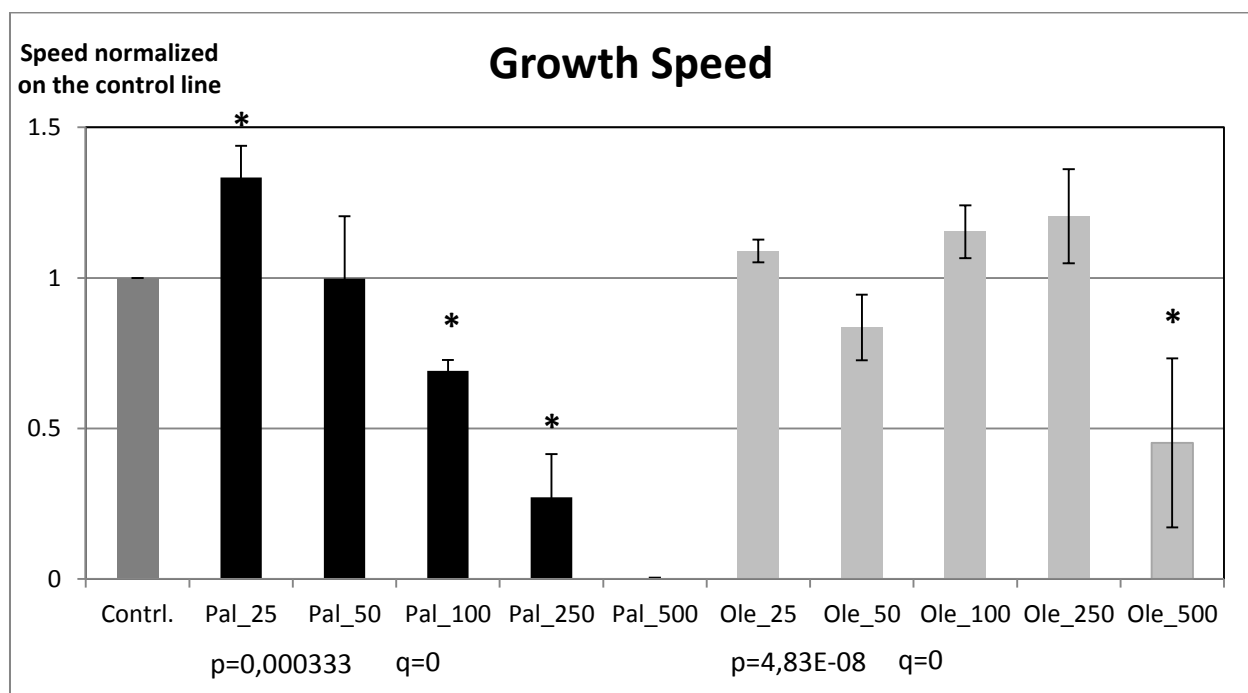


Figure 4 All of the tested conditions are referenced for their growing speed relative to the untreated control lines. The score resulted out of the normalized slope of the linear equation during the exponential growth phase. Interestingly after an initial burst palmitic acid had a negative impact on cellular growth, whereas in the oleic acid treated samples the impact only becomes noticeable at the highest tested concentration. Concentrations marked with a * were found to have significant difference from the control lines in the post hoc test.

Long Term Live Cell Imaging

Long term live cell imaging was performed on a ZEISS spinning disk microscope. Cells were seeded on glass bottom 3cm dishes and transfected with cell light reagents 24 hours prior to image acquisition. This time was sufficient to obtain a decent fluorophore expression and ensure protein stability for the duration of the experiment. Five conditions have been tested so far: oleic acid 100 and 250 μ M, palmitic acid 100 and 250 μ M as well as an untreated control. In each dish multiple positions were picked, which were observed for the next 24 hours. A z-stack acquisition with a step size of 1 μ m was performed each hour at each position. Since mitochondria are very sensitive and prone to fragmentation I employed the fluorescent protein with the longest wavelength and decided against the use of any additional fluorophore to stain the nucleus. To keep laser energy at a minimum the acquisition time per z-plane was increased to 1000ms as a compromise between exposition duration and intensity. A long term imaging of lipid droplets with BodyPI is not possible due to the fact that BodyPI, used for longer durations leads to lipid droplet fusion.

The images are presented as maximum intensity projections to give a good impression of the high connectivity of a healthy mitochondrial system, or respectively the lack of it. The number of replicates are noted in the description for each condition and divided between still living (L) after 24 hours or dead (D). If multiple cells where in the field of view during the experiment, normally all the cells shared the same fate. In the few cases of just one cell surviving whilst the rest died, the result was denoted as dead.

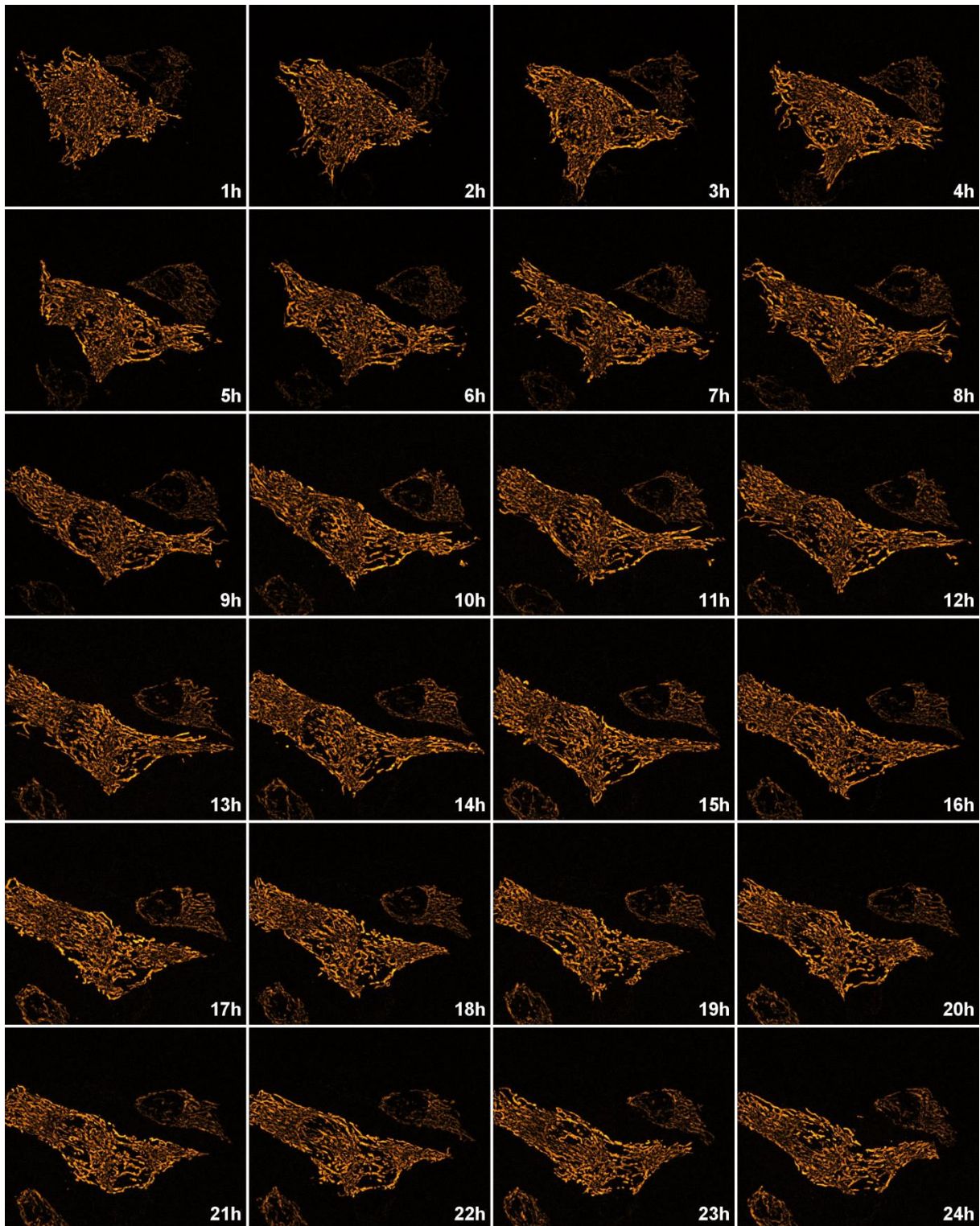


Figure 5 Untreated Control These cells served as my setup control if the treatment is gentle enough to preserve the mitochondrial system in a highly interconnected state. In the case above the two cells in the center of the image, are even a little bit detached due to the prior washing steps, when the acquisition started. But they recovered over the course of the experiment proving that the cells are able to cope with the strain of the lasers. n=11 (L:D=9:2)

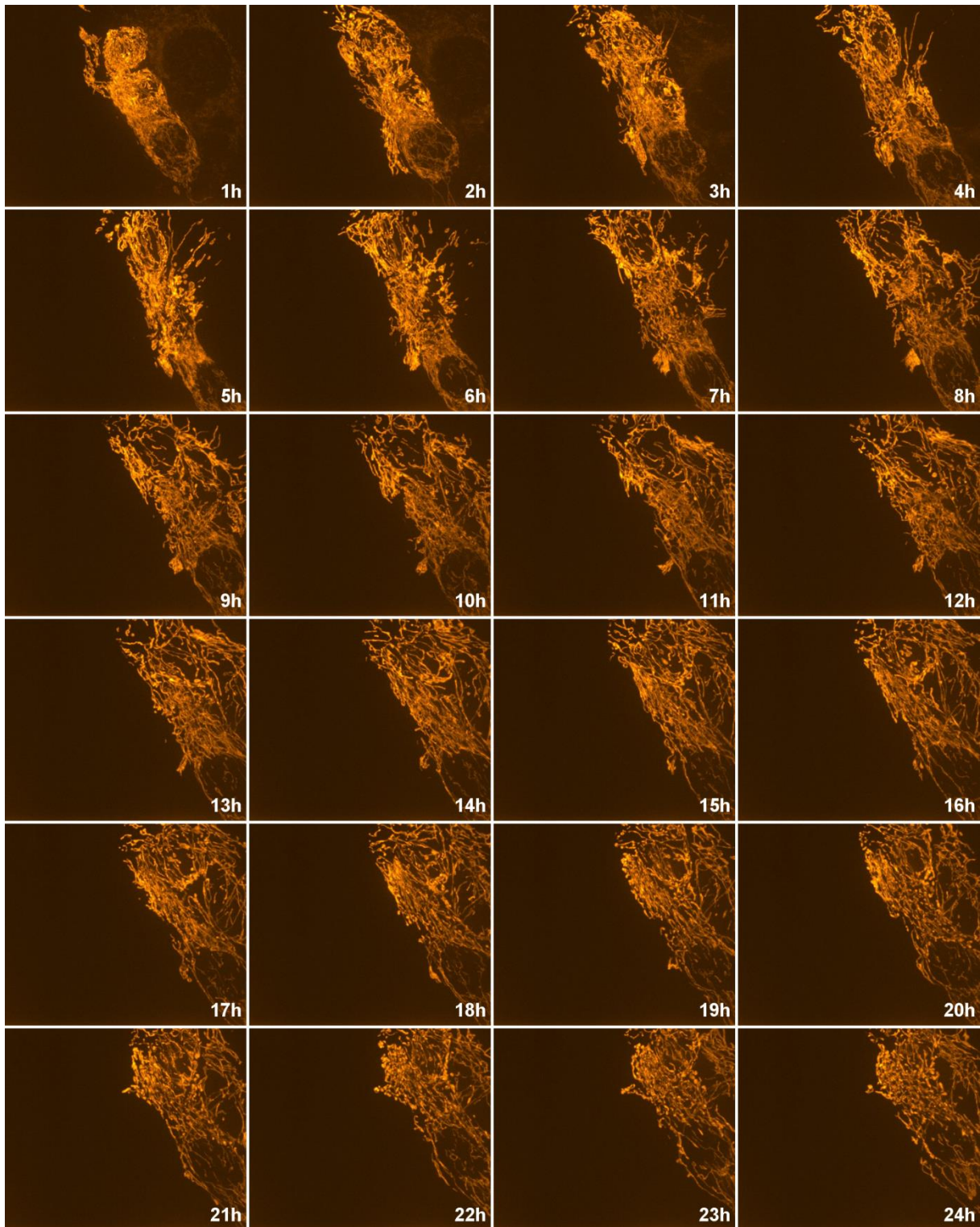


Figure 6 Oleic 100 μ M These cells also started the experiment a little bit detached due to the prior washing steps. Besides drifting out of center they enlarged their mitochondrial system over the course of the experiment. This lipid concentration did definitely not kill the cells, though maybe slowing them down a little bit compared to the control in re-establishing their interconnected mitochondrial system. n=5 (L:D=4:1)

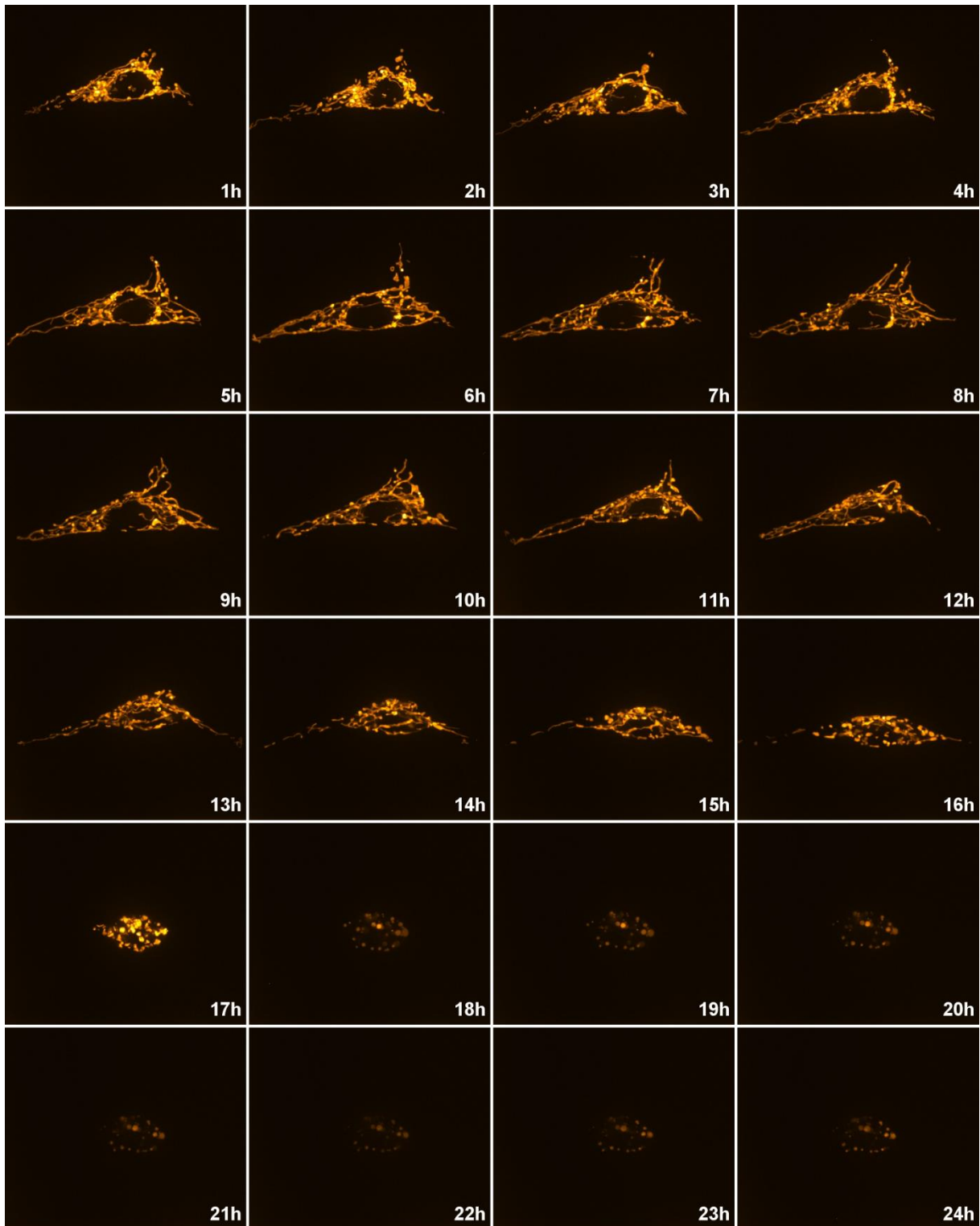


Figure 7 Oleic 250 μ M At this concentration the cell did not survive the whole experiment anymore. Having not suffered as much as the previous shown samples under the washing steps, this cell starts the experiment with a spread out and interconnected mitochondrial network. It improved over the next 8 to 10 hours before at the 12 hour time point starting to show signs of degradation. The network more and more shattered in the following hours. At 17 hours just small and more or less spherical shapes were left and at 18 hours the cell was most likely lysed, explaining the drastic decrease in fluorescence. n=13 (L:D=0:13)

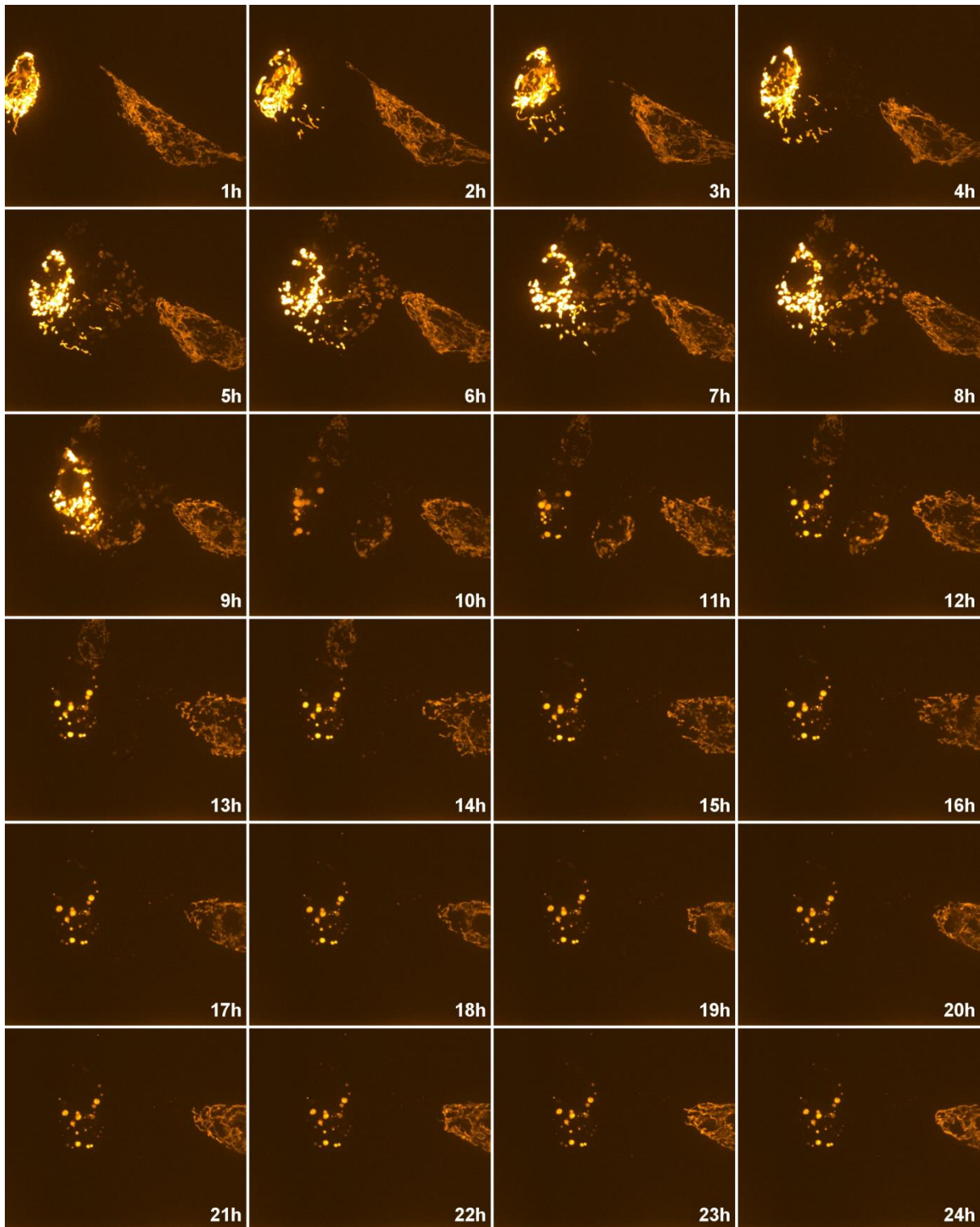


Figure 8 Palmitic 100 μ M There are multiple cells on this image predominantly the one displaying very bright fluorescence on the left hand site and the other two on the right. The cell on the left as well as several others not visible at the beginning of the experiment, started to show signs of mitochondrial fragmentation almost immediately ending up again with these spherical mitochondrial remnants. The two cells on the right did move a little bit out of the image and reduced their network, but they interestingly were the only ones not to die. n=5 (L:D=0:5)

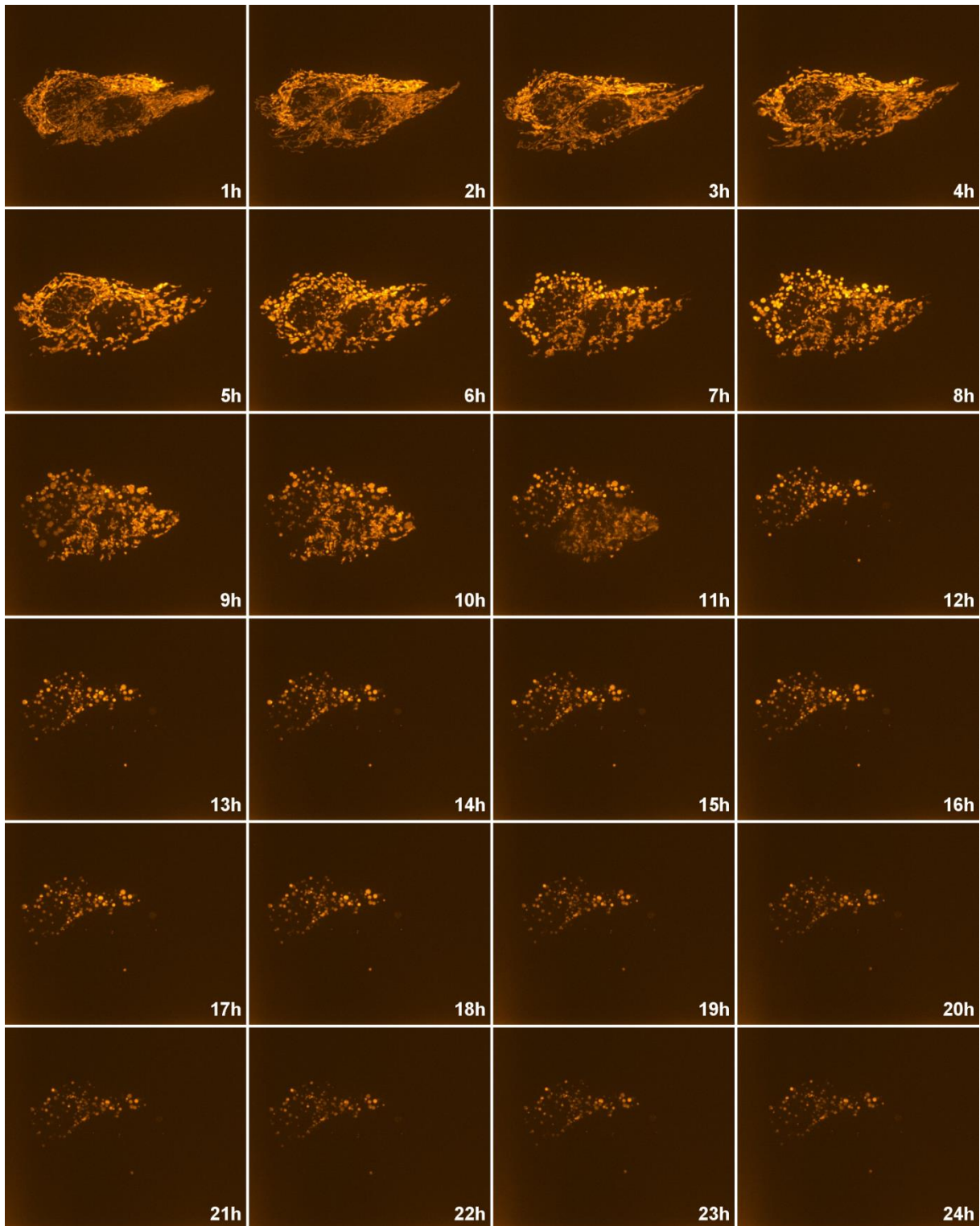


Figure 9 Palmitic 250 μ M These two cells started with immediate fragmentation. The fragmentation of their extended mitochondrial network is observable, until at the 12 hour mark at least one of the two cells definitely lyses. I would not have expected the 250 μ M concentration of palmitic acid to be this noxious for the mitochondrial network, but the effects, in combination with the laser, seem more prominent in all tested conditions. n=10 (L:D=0:10)

Discussion

Without a doubt It can be stated that the impact of oleic and palmitic acid on the cell is of a different kind. The first step in understanding the problem could be found in the inability of the cell to contain palmitic acid within lipid droplets. One study claims that at lower concentration palmitic acid has a superior steatosis inducing effect (Moravcová et al. 2015). This study was performed in primary hepatocytes and they also observed a generally higher tolerance of primary cells than of the HepG2 cells against high fatty acid concentrations. But the only thing I could verify as I tested it myself were the higher toleration levels of the primary cells (data not shown). At a concentration of 25 μ M, where the lipid droplet amount inside the cell is still somewhat comparable between palmitic and oleic acid (Fig.3 B), I was astonished to observe an improved cellular growth rate (Fig.4). Oleic acid did not influence the growth rate, until it hit the point of saturation where no more lipid droplets could be formed. At the point where the cell is unable to form triglycerides out of the free fatty acids the cytotoxic effect started to kick in. In literature the toxic effect of palmitic acid has previously been described, but there are only suggestions concerning its mode of action (Engin und Engin 2017). Palmitic acid, being a saturated fatty acid, is a perfect candidate for beta oxidation. But if beta oxidation runs rampant, radical oxygen species (ROS) will be produced inside the mitochondria in amounts that cannot be tolerated anymore. First mitochondria will react with fragmentation, to reduce their overall activity and if damage due to ROS occurs only small mitochondrial fragments have to be replaced. But if ROS stress reaches a certain level cells start an apoptotic process, most often by mitochondrial outer membrane permeabilization (momp) (Ugarte-Urbe und García-Sáez 2017). If this would be the case it could explain, why I could observe a boost in cell growth in low concentrations of palmitic acid, as it is enough to deliver significant amounts of extra energy and still at a level which redox mechanisms inside the cell can take care of. Verifying this theoretical sequence of events via microscopy is very hard because this process on its own is very dynamic and mitochondria react to any kind of manipulation, whether it is movement of the cells, fixation or the laser of the microscope itself with fragmentation (Archer 2013). So long term live cell imaging was the only option and a spinning disk microscope was perfect for the task spreading the laser over a wider area. Introducing RFP with a baculovirus construct guaranteed a constant expression of the fluorescent protein over 24 hours and the

additional benefit of having basically no unspecific background. But even with this optimized system the introduced stress was enough for the cells to die under conditions that should normally not affect them. The fragmentation happened within 4-6 hours and was rarely followed by instant cell death, but instead the mitochondrial fragments formed spherical shapes. This could be due to the damage initiating the formation of mitophagosomes, a process that occurs if the cell tries to get rid of dysfunctional mitochondria. A study published in 2017 identified a mechanism, how ROS accumulation, due to high glucose levels, leads to Zn^{2+} mediated fission of mitochondria by dynein related protein 1 (DRP-1) recruitment (Abuarab et al. 2017). A Ca^{2+} flux through the transient receptor membrane channel subtype melastatin 2 (TRPM2) after ROS activation leads to the freeing of Zn^{2+} from lysosomes. If the same signaling happens in HepG2 cells, chelating the Ca should prevent the mitochondria from fractioning. I was not able to observe any amelioration of the crippling effects induced by palmitic acid (data not shown), though a similar process has been suggested in another organism (Kumari et al. 2017). An alternative explanation why palmitic acid has this noxious impact could be that it is tunneled into ceramide synthesis. Scientists know that ceramides, like palmitic acid, become toxic at elevated levels, but are unsure why exactly (Engin und Engin 2017). Biophysicists suggested a model wherein theoretically a surplus of ceramides could self-assemble into a channel structure and cooperate into intracellular membrane structures (Anishkin et al. 2006). This hypothesis would also explain why there are basically no lipid droplets formed from palmitic acid and why the difference between palmitic and oleic acid in affecting the cell is that dramatic. I decided to use two inhibitors to block essential steps in the sphingolipid biosynthesis pathway. The first, myriocin, inhibits the *serine palmitoyltransferase*, the second, Fumisin B₁, inhibits the *ceramide synthase*. But the tests with both inhibitors turned out inconclusive (data not shown). But I will omit neither theory yet because most of the tests I could perform were one-time experiments with only few concentrations due to time constrains.

Not only are mitochondria essential for every cell in our body, so is their constant fragmentation, renewal and reattaching to the network (Friedman und Nunnari 2014; Jon Lieff 2014b, 2014a). With too many liver cells dying, an inflammatory process will start, and this is what will progress a simple NAFL into NASH and even further. It has been published that it is possible to counter the toxic effects of palmitic acid by addition of oleic acid, but it

is still not understood why (Leamy et al. 2016; Moravcová et al. 2015; Plötz et al. 2016). So the old piece of advice, to stay away from the cheap unhealthy saturated fatty acids and to make sure to get enough healthy unsaturated fatty acids, might still be the best advice today.

Conclusion and Perspectives

Though palmitic and oleic acid have been used in the past to induce steatosis in experimental setups, their cellular effects differed markedly in all my experiments. Oleic acid treatment proofed to be an efficient way to induce steatosis in the HepG2 cells in a dose dependent fashion, whereas palmitic acid failed to increase the lipid droplet amount beyond an initial level. Also oleic acid did not influence the cell growth besides the highest tested concentration of 500 μ M. Palmitic acid, on the contrary, displayed immediate influence on the growth rate. Intriguingly, the lowest concentration of 25 μ M led to a 30% acceleration of growth. At 50 μ M the growth rate returned to normal, continuing the decline until reaching zero at 500 μ M. The initial growth improvement offered by the saturated fatty acid may be due to enhanced beta oxidation (which requires saturated fatty acids as substrates), the descending effect could be attributed to ROS accumulation and/or increased ceramide synthesis which may lead to apoptosis. Investigating the mitochondrial system proofed to be a formidable challenge because the experimental setup influenced the viability negatively and lead to cell death even at concentrations that should have had no influence according to the growth curves.

At this point I established a solid foundation for future research on the mechanism of noxious fatty acid specific cellular effects. The lipid droplet quantification program has received a major upgrade in the moment when I changed the mode of analysis from 2D into 3D. This will finally solves the problem of different lipid droplet morphologies that can occur through the treatments with different fatty acids. With the right algorithms for a proper deconvolution and appropriate acquisition settings, in the future it will not only be possible to get information about the volume but it will include information about size distribution and number of individual droplets. A verification of the program in the first place, through neutral lipid quantification will be needed.

I am aware of the fluorescent sensors that exist for radical oxygen species and also performed some measurements with the MitoSOX reagent. But at this state of my research I managed to set up a working protocol but the sample size used for the preliminary experiment was too small to make a qualified statement. I am going to set up an experiment with a relative quantification via FACS, which supports a bigger sample size as well as time resolved measurements. The same is true for the membrane potential, which will be measured with the JC1 dye.

During my time writing down this thesis I had the opportunity to work in addition with myristic acid incubated cells and measure their lipid droplet content. Since myristic acid is the C14 saturated fatty acid, I expected it to behave more like palmitic acid than oleic acid. But surprisingly I could observe that the cells did not have any problem storing this fatty acid in lipid droplets. This somewhat implies that enhanced beta oxidation and thus elevated ROS levels cannot be the sole culprit for the toxicity of palmitic acid, otherwise myristic acid treatment should have shown some similarities.

Mitochondria are not only susceptible to influences on their dynamics but also to changes of their lipid composition (Mårtensson et al. 2017). The excess of palmitic acid could lead to changes in their membrane composition and slow down their productiveness. This should manifest itself in a drop of membrane potential.

To improve on the data gathered from the long term live cell imaging I am currently working on a program that tracks the junction points of the mitochondrial system over time and in 3D. The resulting output should provide information about how many junctions have been formed and broken at every measured time point and thus be a representative readout.

Acknowledgements

My sincerest gratitude belongs to Ms Ruth Birner-Grünberger and her team, which have supported me all the time and provided me with everything I needed. The caring and friendly atmosphere in this group lets you feel right at home and is exactly what turns tedious and repetitive laboratory work into passion for your future job. I also want to thank Markus and Kristin from the ZMF core facility imaging for their continuous support and maintenance of the microscopes. Naturally the same goes for Roland Malli and his group who provided me with access to the Nipkow microscope.

Literaturverzeichnis

Abuarab, Nada; Munsey, Tim S.; Jiang, Lin-Hua; Li, Jing; Sivaprasadarao, Asipu (2017): High glucose-induced ROS activates TRPM2 to trigger lysosomal membrane permeabilization and Zn²⁺-mediated mitochondrial fission. In: *Science signaling* 10 (490). DOI: 10.1126/scisignal.aal4161.

Adams, L. A.; Angulo, P. (2006): Treatment of non-alcoholic fatty liver disease. In: *Postgraduate medical journal* 82 (967), S. 315–322. DOI: 10.1136/pgmj.2005.042200.

Anishkin, A.; Sukharev, S.; Colombini, M. (2006): Searching for the molecular arrangement of transmembrane ceramide channels. In: *Biophysical journal* 90 (7), S. 2414–2426. DOI: 10.1529/biophysj.105.071977.

Archer, Stephen L. (2013): Mitochondrial dynamics--mitochondrial fission and fusion in human diseases. In: *The New England journal of medicine* 369 (23), S. 2236–2251. DOI: 10.1056/NEJMr1215233.

Campbell, Neil A.; Reece, Jane B.; Kratochwil, Anselm; Lazar, Thomas (Hg.) (2012): *Biologie*. 8., aktualisierte Aufl., korr. Nachdruck von 2012. München: Pearson Studium (Pearson Studium - Biologie).

Centers for Disease Control and Prevention (2016): Chronic Liver Disease and Cirrhosis. Online verfügbar unter <https://www.cdc.gov/nchs/fastats/liver-disease.htm>, zuletzt aktualisiert am 06.10.2016, zuletzt geprüft am 20.06.2018.

- Clark, Jeanne M.; Diehl, Anna Mae (2003): Nonalcoholic fatty liver disease. An underrecognized cause of cryptogenic cirrhosis. In: *JAMA* 289 (22), S. 3000–3004. DOI: 10.1001/jama.289.22.3000.
- Engin, Ayse Basak; Engin, Atilla (2017): Obesity and Lipotoxicity. Cham: Springer International Publishing (Advances in Experimental Medicine and Biology, v.960). Online verfügbar unter <https://ebookcentral.proquest.com/lib/gbv/detail.action?docID=4872963>.
- Friedman, Jonathan R.; Nunnari, Jodi (2014): Mitochondrial form and function. In: *Nature* 505 (7483), S. 335–343. DOI: 10.1038/nature12985.
- Horton, Horace Robert; Moran, Laurence A.; Scrimgeour, K. Gray; Perry, Marc D.; Rawn, J. David; Biele, Carsten (Hg.) (2008): Biochemie. 4., aktualisierte Aufl. München: Pearson Studium (bio - Biologie).
- Johnson, Iain (2010): The molecular probes handbook. A guide to fluorescent probes and labeling technologies. 11. ed. Carlsbad, Calif.: Life Technologies.
- Jon Lieff, M. D. (2014a): Intelligent Mitochondria Communication with Neurons. Online verfügbar unter <http://jonlieffmd.com/blog/intelligent-mitochondria-communication-with-neurons>, zuletzt geprüft am 14.01.2018.
- Jon Lieff, M. D. (2014b): Dynamic Relationship of Mitochondria and Neurons. Online verfügbar unter <http://jonlieffmd.com/blog/dynamic-relationship-of-mitochondria-and-neurons>, zuletzt geprüft am 14.01.2018.
- Karbowski, Mariusz (2010): Mitochondria on Guard. Role of Mitochondrial Fusion and Fission in the Regulation of Apoptosis. In: Claudio Hetz (Hg.): BCL-2 Protein Family. Essential Regulators of Cell Death, Bd. 687. New York, NY: Landes Bioscience and Springer Science+Business Media LLC (Advances in Experimental Medicine and Biology, 687), S. 131–142.
- Kumari, Anjali; Singh, Krishn Pratap; Mandal, Abhishek; Paswan, Ranjeet Kumar; Sinha, Preeti; Das, Pradeep et al. (2017): Intracellular zinc flux causes reactive oxygen species mediated mitochondrial dysfunction leading to cell death in *Leishmania donovani*. In: *PLoS one* 12 (6), e0178800. DOI: 10.1371/journal.pone.0178800.

Leamy, Alexandra K.; Hasenour, Clinton M.; Egnatchik, Robert A.; Trenary, Irina A.; Yao, Cong-Hui; Patti, Gary J. et al. (2016): Knockdown of triglyceride synthesis does not enhance palmitate lipotoxicity or prevent oleate-mediated rescue in rat hepatocytes. In: *Biochimica et biophysica acta* 1861 (9 Pt A), S. 1005–1014. DOI: 10.1016/j.bbalip.2016.05.013.

Mårtensson, Christoph U.; Doan, Kim Nguyen; Becker, Thomas (2017): Effects of lipids on mitochondrial functions. In: *Biochimica et biophysica acta* 1862 (1), S. 102–113. DOI: 10.1016/j.bbalip.2016.06.015.

Moravcová, A.; Červinková, Z.; Kučera, O.; Mezera, V.; Rychtrmoc, D.; Lotková, H. (2015): The effect of oleic and palmitic acid on induction of steatosis and cytotoxicity on rat hepatocytes in primary culture. In: *Physiological research* 64 Suppl 5, S627-36.

Penzlin, Heinz; Beinbrech, Gernot (Hg.) (2009): Lehrbuch der Tierphysiologie. 7., neu bearb. und erw. Aufl., unveränd. Nachdr. Heidelberg: Spektrum Akad. Verl.

Perseus Software (2017). Online verfügbar unter <http://www.coxdocs.org/doku.php?id=perseus:start>, zuletzt aktualisiert am 21.07.2017, zuletzt geprüft am 16.07.2018.

Plötz, Thomas; Hartmann, Magnus; Lenzen, Sigurd; Elsner, Matthias (2016): The role of lipid droplet formation in the protection of unsaturated fatty acids against palmitic acid induced lipotoxicity to rat insulin-producing cells. In: *Nutrition & metabolism* 13, S. 16. DOI: 10.1186/s12986-016-0076-z.

Rinella, Mary E. (2015): Nonalcoholic fatty liver disease. A systematic review. In: *JAMA* 313 (22), S. 2263–2273. DOI: 10.1001/jama.2015.5370.

Rutkowski, Joseph M.; Stern, Jennifer H.; Scherer, Philipp E. (2015): The cell biology of fat expansion. In: *The Journal of cell biology* 208 (5), S. 501–512. DOI: 10.1083/jcb.201409063.

Schindelin, Johannes; Arganda-Carreras, Ignacio; Frise, Erwin; Kaynig, Verena; Longair, Mark; Pietzsch, Tobias et al. (2012): Fiji. An open-source platform for biological-image analysis. In: *Nature methods* 9 (7), S. 676–682. DOI: 10.1038/nmeth.2019.

Schönfeld, Peter; Wieckowski, Mariusz R.; Lebidzińska, Magdalena; Wojtczak, Lech (2010): Mitochondrial fatty acid oxidation and oxidative stress. Lack of reverse electron transfer-

associated production of reactive oxygen species. In: *Biochimica et biophysica acta* 1797 (6-7), S. 929–938. DOI: 10.1016/j.bbabi.2010.01.010.

Scott, Iain; Youle, Richard J. (2010): Mitochondrial fission and fusion. In: *Essays in biochemistry* 47, S. 85–98. DOI: 10.1042/bse0470085.

Seahorse Bioscience (2010): Preparation of Bovine Serum Albumin (BSA)-Conjugated Palmitate. A substrate for measuring fatty acid oxidation [FAO] in the XF Analyzer. Online verfügbar unter <https://www.google.at/url?sa=t&rct=j&q=&esrc=s&source=web&cd=1&ved=0ahUKEwisjuvdxdfYAhVRJVAKHbXWBdsQFggrMAA&url=https%3A%2F%2Fwww.researchgate.net%2Ffile.PostFileLoader.html%3Fid%3D53913148d2fd64f7568b4594%26assetKey%3DAS%253A273541168074752%25401442228704111&usg=AOvVaw1LrJ2IjGY64klyJtY3EX-T>, zuletzt aktualisiert am 15.10.2010, zuletzt geprüft am 14.01.2018.

Speijer, D.; Manjeri, G. R.; Szklarczyk, R. (2014): How to deal with oxygen radicals stemming from mitochondrial fatty acid oxidation. In: *Philosophical transactions of the Royal Society of London. Series B, Biological sciences* 369 (1646), S. 20130446. DOI: 10.1098/rstb.2013.0446.

Springer; Pawley, James B. (Hg.) (2006): Handbook of biological confocal microscopy. 3. ed. New York, NY: Springer.

Ugarte-Urbe, Begoña; García-Sáez, Ana J. (2017): Apoptotic foci at mitochondria. In and around Bax pores. In: *Philosophical transactions of the Royal Society of London. Series B, Biological sciences* 372 (1726). DOI: 10.1098/rstb.2016.0217.

World Health Organisation: Age-standardized death rates of liver cirrhosis. Online verfügbar unter http://www.who.int/gho/alcohol/harms_consequences/deaths_liver_cirrhosis/en/, zuletzt geprüft am 26.06.2018.